Neurobiology of Disease 144 (2020) 105030

Contents lists available at ScienceDirect

Neurobiology of Disease

journal homepage: www.elsevier.com/locate/ynbdi

Neurofibromatosis 1 - Mutant microglia exhibit sexually-dimorphic cyclic AMP-dependent purinergic defects

Nirmeen Elmadany[a,d,1], Francesca Logiacco[a,d,1], Alice Buonfiglioli[a,c], Verena C. Haage[a], Elizabeth C. Wright-Jin[b], Alexander Schattenberg[a], Roxane M. Papawassiliou[a], Helmut Kettenmann[a,*,2], Marcus Semtner[a,2,*], David H. Gutmann[a,b,*,2]

[a] Cellular Neurosciences, Max-Delbrück-Center for Molecular Medicine in the Helmholtz Association, 13125 Berlin, Germany
[b] Department of Neurology, Washington University School of Medicine, St. Louis, MO 63110, USA
[c] Institute of Cell Biology and Neurobiology, Charité – Universitätsmedizin Berlin, corporate member of Freie Universität Berlin, Humboldt-Universität zu Berlin, and Berlin Institute of Health, 10117 Berlin, Germany
[d] Department of Biology, Chemistry, and Pharmacy, Freie Universität Berlin, 12169 Berlin, Germany

ARTICLE INFO

Keywords:
Brain
Neurofibromin
P2RY12
Purinergic signaling
Sex differences
Microglia
cAMP

ABSTRACT

As critical regulators of brain homeostasis, microglia are influenced by numerous factors, including sex and genetic mutations. To study the impact of these factors on microglia biology, we employed genetically engineered mice that model Neurofibromatosis type 1 (NF1), a disorder characterized by clinically relevant sexually dimorphic differences. While microglia phagocytic activity was reduced in both male and female heterozygous *Nf1* mutant (*Nf1*+/−) mice, purinergic control of phagocytosis was only affected in male *Nf1*+/− mice. ATP-induced P2Y-mediated membrane currents and P2RY12-dependent laser lesion-induced accumulation of microglial processes were also only impaired in male, but not female *Nf1*+/−, microglia. These defects resulted from *Nf1*+/− male-specific defects in cyclic AMP regulation, rather than from changes in purinergic receptor expression. Cyclic AMP elevation by phosphodiesterase blockade restored the male *Nf1*+/− microglia defects in P2Y-dependent membrane currents and process motility. Taken together, these data establish a sex-by-genotype interaction important to microglia function in the adult mouse brain.

1. Introduction

The implementation of precision medicine requires the identification of the risk factors that underlie disease pathogenesis and progression (Wegscheid et al., 2018; Bennett and Bennett, 2020; Yirmiya et al., 2015; Wright-Jin and Gutmann, 2019). In the setting of central nervous system (CNS) disease, microglia have emerged as one of the key cell types important for modifying pathobiology and integrating risk factors. As such, microglia serve important functions in the development and evolution of numerous CNS disorders, ranging from autism to Alzheimer's disease (Wolf et al., 2017; Whitelaw, 2018). In addition to actively participating in disease pathogenesis, risk factors, such as the germline mutation (e.g., ApoE status, Krasemann et al., 2017) and sex (Hanamsagar et al., 2017; McCarthy and Wright, 2017; Guneykaya et al., 2018), alter microglia function. In this regard, sexually dimorphic differences in microglia function can impact on CNS disease development (Vegeto et al., 2020; Kerr et al., 2019; Fisher et al., 2018; Nissen, 2017).

To explore the impact of germline genetics and sex in the setting of a common neurodevelopmental disorder characterized by microglia dysfunction, we focused on the monogenic syndrome, Neurofibromatosis type 1 (NF1). Caused by germline mutations in the *NF1* gene, children with NF1 are prone to brain tumours, in particular, optic pathway gliomas (OPGs), and autism, as well as learning disabilities, attention deficits, and motor function delays (Gutmann et al., 2017). Moreover, some of these CNS phenotypes are sexually dimorphic: whereas autism is more common in male in the general population, this male predominance is dramatically attenuated in children with NF1 (Morris et al., 2016). Similarly, girls with NF1-OPGs are 3- to 5-times more likely than boys to lose vision from their tumours and require treatment (Diggs-Andrews et al., 2014b; Diggs-Andrews et al., 2014a). In *Nf1* optic glioma mice, this sex-specific effect operates at the

* Corresponding authors.
E-mail addresses: kettenmann@mdc-berlin.de (H. Kettenmann), marcus.semtner@mdc-berlin.de (M. Semtner), gutmannd@wustl.edu (D.H. Gutmann).
[1] The first two authors contributed equally to this study.
[2] The last three authors contributed equally to this study.

https://doi.org/10.1016/j.nbd.2020.105030
Received 20 May 2020; Received in revised form 9 July 2020; Accepted 23 July 2020
Available online 29 July 2020

level of microglia, where estrogen binding to the estrogen receptor-beta on microglia underlies the observed retinal ganglion cell loss, nerve fibre layer thinning, and visual acuity reduction (Toonen et al., 2017).

To explore additional sex-specific differences uncovered by *Nf1* mutation, we leveraged *Nf1* mutant mice, genetically similar to patients with NF1 harboring one mutant germline *Nf1* allele. We identified male-specific defects in purinergic function, including phagocytosis, process movement, and ATP induced membrane currents, which result from impaired cyclic AMP signaling. Collectively, these findings establish sex-by-genotype microglial abnormalities in the setting of *Nf1* mutation.

2. Materials and methods

2.1. Ethics statement

All procedures involving the handling of living mice were performed in strict accordance with the German Animal Protection Law, and were approved by the Regional Office for Health and Social Services in Berlin (Landesamt für Gesundheit und Soziales, Berlin, Germany, Permit Number T0014/08, X9023/12, X9005/18, A0376/17) and the Washington University Animal Studies Committee. Adult mice were euthanized by cervical dislocation or by transcardial perfusion of PBS or PFA after intraperitoneal injection of pentobarbital (Narcoren, Merial GmbH, Hallbergmoos, Germany). All efforts were made to minimize suffering.

2.2. Mice

Wild type and *Nf1*+/− (Brannan et al., 1994) mice used in this study, either bred onto a wild type or MacGreen (Csf1r-eGFP; Sasmono et al., 2003) C57/BL6 background, were kept under a 12 h/12 h dark-light cycle with food and water supply ad libitum, in accordance with German laws for animal protection.

2.3. Acute brain slice preparation

Acute cortical brain slices were prepared as previously described (Boucsein et al., 2003). In brief, mice were euthanized by cervical dislocation, and their brains removed and cooled in ice-cold artificial cerebrospinal fluid (aCSF) containing (in mM): 230 Sucrose, 2.5 KCl, 10 $MgSO_4$, 0.5 $CaCl_2$, 1.25 NaH_2PO_4, 26 $NaHCO_3$, and 10 D-glucose, pH 7.4; gassed with 95% O_2/ 5% CO_2. Brains were then mounted on a vibratome (HM650V, Thermo Scientific, Massachusetts, USA), and 250 μm thick coronal brain slices were generated and kept at room temperature for experiments for up to 5 h in gassed ACSF containing (in mM): 134 NaCl, 2.5 KCl, 1.3 $MgCl_2$, 2 $CaCl_2$, 1.26 K_2HPO_4, 26 $NaHCO_3$, and 10 D-glucose (pH 7.4). Acute brain slices were used for patch clamp recordings and in situ 2-photon live-cell imaging.

2.4. Immunohistochemistry, confocal microscopy and microglial density analysis

For the immunohistochemical analysis, animals were deeply anesthetized with ketamine, perfused with phosphate buffered saline (PBS) solution, followed by 4% PFA in PBS. Afterwards, mice were decapitated, and their brains removed and sectioned in the coronal plane at 40 μm thickness using a sliding dry-iced-cooled microtome. Free-floating sections were incubated for 1 h in 5% donkey serum and 0.1% Triton-X in Tris-buffered saline solution (TBSplus).

For microglial density analysis, goat anti-Iba1 (Abcam, ab5076) primary antibody was diluted 1:250 in TBS plus and incubated overnight at 4 °C. The secondary antibody, donkey anti-goat Alexa Fluor 488 (Dianova, 705–545-147), was also prepared in TBS plus at a dilution of 1:200, and cell nuclei were labeled using 4′,6-diamidino-2-phenylindole (DAPI, Dianova) at a dilution of 1:200, for two hours at room temperature. Sections were subsequently mounted in Aqua Polymount on glass slides for analysis.

Images were acquired using a confocal microscope equipped with a 10× objective and LASAF software (Leica TCS SPE, Leica microsystem). Pictures were taken throughout the entire thickness of the slice by z-stacking (3 μm z-step size, 13 steps).

The number of microglia cells per mm^2 was quantified using Fiji ImageJ software followed by analysis with Cell Profiler® automated cell counter software (https://cellprofiler.org/). A total of four slices per brain region and animal were analyzed. Briefly, the desired areas of interest (brain region) were selected in Image J on the the maximum intensity z-projection of the confocal scans. Channels were split into separate TIF images for analysis with a modified cell profiler protocol (Bloomfield et al., 2018). Microglial cell number was quantified using modified parameters, including typical diameter object sizes between 0.5 and 50, and a lower threshold value of 0.35. For the DAPI channel, the diameter object size was set to 10–50 (arbitrary units). A further filter step that incorporates microglial cell body size was set to 25. Once extrapolated, the microglia counts in the different brain regions, the average of four independent images, were normalized, based on the quantified area in mm^2. Data are presented as number of microglia cells/mm^2.

2.5. Adult microglia cultures

Microglia from (12–16 weeks old) adult mice were prepared as described previously (Pannell et al., 2016). Briefly, brains obtained from adult male and female WT and *Nf1*+/− mice (12–16 weeks) were freed of blood vessels and meninges, mechanically dissociated, and digested with trypsin and DNAse. Cells were then plated onto a confluent monolayer of P0-P2 WT astrocytes in 75 cm^2 flasks. The feeder astrocyte layer was depleted of neonatal microglial cells using chlodronate (200 μg/ml) before adding microglia. Mixed adult and neonatal microglial cultures were maintained in fresh complete DMEM, and the medium changed every third day, followed by addition of 33% L292-conditioned medium at day 7. One week later, cells were shaken off, and used for experiments within 24–48 h.

2.6. In situ phagocytosis assay

The phagocytosis assay was performed as previously described (Wendt et al., 2017; Pan et al., 2018). Briefly, 130 μm acute coronal brain slices from 14 to 16 week-old *Nf1*+/− mice and their WT littermates (n = 5–6, for AR-C66096 condition n = 2–3) were used. Brains were sliced in ice-cold ACSF buffer solution containing (in mM): NaCl, 134; KCl, 2.5; $MgCl_2$, 1.3; $CaCl_2$, 2; K_2HPO_4, 1.25; $NaHCO_3$, 26; D-glucose, 10; pH 7.4; gassed with 95% O_2 and 5% CO_2 using a vibratome (HM650V, Thermo Scientific, Massachusetts, USA). Slices rested for 2 h at room temperature in ACSF, which was constantly gassed with carbogen (95% O_2 and 5% CO_2). The slices were subsequently incubated for 1 h at 37 °C (95% O_2 / 5% CO_2) with Bright Blue fluorescent carboxylated microspheres (4.5 μm diameter, Polysciences, Hirschberg an der Bergstraße, Germany) to allow for phagocytosis (with the corresponding chemicals to the included conditions). Prior to incubation, microspheres were opsonized by shaking in FCS at 1000 rpm for 30 min at room temperature and centrifuged (2 min at 3000 rpm, Eppendorf Centrifuge 5417R- Rotor FA45–30-11; rotor radius metric: 9.5 cm), washed in PBS and resuspended in HBSS. Each brain slice was incubated with 2.45 × 10^6 microspheres with a 4.5 μm diameter in a volume of 500 μl HBSS. UDP (100 μM), MRS2578 (5 μM) or AR-C66096 (1 μM) were added to the HBSS-microsphere suspension during the 1 h incubation period. Brain slices were washed after microsphere treatment 3 × 20 min in 0.1 M PBS at pH 7.4, fixed with 4% PFA for 1 h at room temperature, and then stored at 4 °C. For staining with Iba1, fixed slices were incubated for 4 h at room temperature in blocking buffer containing 2% Triton X-100, 2% bovine serum albumin and 10%

donkey serum in 0.1 M PBS, pH 7.4. First, incubation with goat polyclonal anti-Iba1 antibody (1:600, Abcam, Berlin, Germany) was performed overnight at 4 °C in staining buffer (1:10 dilution of blocking buffer in 0.1 M PBS pH 7.4). Slices were incubated with secondary antibody (1:250 in staining buffer; Alexa Fluor 647-labeled donkey anti-goat antibody; Invitrogen, Karlsruhe, Germany) for 2 h at room temperature following 3 × 20 min washes in 0.1 M PBS, pH 7.4. Slices were mounted in Aqua-Poly/Mount (Polysciences). For confocal imaging of microglia and microspheres, cortical view fields were randomly chosen within the cortex, 21 µm thick z-stacks at 1.05 µm intervals beginning from the surface of each slice were acquired. We used a confocal laser-scanning microscope from Leica (TCS SPE) and a 20× oil immersion objective. Data analysis to assess microglial phagocytic activity was performed using Imaris 9.1 (Bitplane, Zürich, Switzerland). The $Iba1^+$ cell volumes of high-resolution SPE confocal microscopy stacks were 3D surface-rendered after "background subtraction" (1–3 times; 90 µm each) and thresholding using values of 25–40. Detection of microspheres within the rendered $Iba1^+$ cell volume was performed automatically by the "split into surface object" plug-in. The phagocytic index (PI) was calculated by the following equation: $n_{PM}*10^4/V_{Iba1}$ where n_{PM} is the number of phagocytosed microspheres and V_{Iba1} is the volume of Iba1 fluorescence in μm^3. The student's *t*-test was used to compare each condition separately between *Nf1*+/− and WT groups.

2.7. Electrophysiological recordings

Conventional patch-clamp amplifiers were used (EPC9 and EPC10, HEKA Elektronik, Lambrecht, Germany). Acute 250 µm coronal brain slices were prepared from *Nf1*+/− and wild type mice generated on a MacGreen background (Sasmono and Williams, 2012) for microglia identification by fluorescence on an epifluorescent microscope. Patch pipettes were pulled from borosilicate glasses and had resistances of 4–6 MΩ. The following intracellular solution was used (in mM): KCl, 130; $MgCl_2$, 2; $CaCl_2$, 0.5; Na-ATP, 2; EGTA, 5; HEPES, 10 and sulforhodamine 101, 0.01 (Sigma Aldrich,) and had an osmolarity of 280–290 mOsm/L adjusted to a pH of 7.3 with KOH. The extracellular solution contained (in mM): NaCl, 134; KCl, 2.5; $MgCl_2$, 1.3; $CaCl_2$, 2; K_2HPO_4, 1.25; $NaHCO_3$, 26; D-glucose, 10; pH 7.4; 310–320 mOsm/L and was gassed with carbogen (95% O_2/ 5% CO_2). Experiments with series resistances less than ~65 MΩ were used for data analysis. All experiments were performed in the voltage-clamp configuration. To obtain current-voltage curves during continuous recordings, the membrane was clamped every 5 s from a holding potential of −70 or − 20 mV (basal current and ATP-induced current, respectively) to a series of de- and hyperpolarizing voltages ranging from −140 mV to 60 mV with 20 mV increment, 100 ms in duration. Membrane currents were averaged for quantification between 30 and 45 ms after clamping the membrane to a given value from the resting potential. Membrane capacitance was quantified based on an exponential fit of the current decay in response to a − 10 mV test pulse. The same pulse was used to quantify series resistance from the peak amplitude of the membrane capacitance currents. Comparisons of membrane currents between different groups were always normalized to the membrane capacitance.

2.8. Two-photon imaging and laser lesioning

Live imaging of microglial processes was performed on 250 µm coronal brain slices from *Nf1*+/− mice and their WT littermates maintained on a MacGreen background (Sasmono and Williams, 2012) using a custom-built two-photon laser-scanning microscope (Till Photonics, Gräfelfing, Germany). EGFP was excited by a Chameleon Ultra II laser (Coherent, Dieburg, Germany) at a wavelength of 940 nm. A 40× water-immersion objective (NA 0.8, Olympus, Hamburg, Germany) was used, with scanned 60 µm thick z-stacks and a step size of 3 µm covering a field of 384 × 384 μm^2. Laser lesions were set to 40 µm under the slice surface in the cortex by focusing the laser beam, set to a wavelength of 810 nm and to maximum power in the selected imaging volume, and scanned the tissue until autofluorescence of the injured tissue was visible. This procedure resulted in lesions of ~ 20 µm in diameter in the middle of the observed region. IGOR Pro 6.37 (Lake Oswego, USA) was used for data analysis as in Davalos et al. (2005). The sequences of 3D image stacks were converted into sequences of 2D images by a maximum intensity projection algorithm. Grayscale images were first converted into binary form using a threshold. For quantification, microglial response to focal lesion was defined as EGFP+ pixel count in a proximal circular region 45 µm around the lesion site over time (Rx(t)). Distal fluorescence of the first time point was determined within a diameter of 45 µm to 90 µm around the lesion site for normalization (Ry(0)). Microglial responses are were represented as R (t) = (Rx(t)-Rx(0))/Ry(0).

2.9. Microglia isolation by MACS

12–16 week male and female *Nf1*+/− and WT mice (n = 3 each) were transcardially perfused with ice-cold Phosphate Buffered Saline (PBS) to harvest the brain. Brains were subsequently homogenized at 0–4 °C in dissection buffer (HBSS, 45% glucose, 1 M HEPES) and cell pellets were resuspended in 25 ml of 22% Percoll (GE Healthcare, Little Chalfont, UK). The volume of 5 ml PBS was added as a layer on top. Centrifugation was performed for 20 min at 950 g with medium acceleration and no brakes to remove myelin and debris. Pellets were resuspended in ice-cold MACS buffer and incubated with anti-mouse CD11b antibodies coupled to magnetic beads (Miltenyi Biotech, Bergisch Gladbach, Germany) for 15 min at 4 °C. Cells were resuspended in MACS buffer and passed through medium-sized MACS columns (Miltenyi Biotech) attached to a magnet. The flow-through was discarded and the cells were flushed out of the columns in MACS buffer, collected by centrifugation, and stored at −80 °C for cAMP ELISA or seeded in a 96 well plate for the cell viability assay.

2.10. RT-qPCR

Total RNA was extracted from acutely isolated microglia by MACS using ReliaPrep RNA Miniprep System (Promega, Madison, Wisconsin, USA). cDNA synthesis was performed using the PrimeScript™ RT reagent Kit (Takara, Kusatsu, Shiga, Japan). Quantitative real-time PCR reactions to amplify 1 ng of total cDNA were performed in a 7500 Fast Real-Time thermocycler (Applied Biosystems, Carlsbad, USA) using the SYBR Select Master Mix (Applied Biosystems). CT values were normalized using Hypoxanthin-Guanin-Phosphoribosyl-Transferase 1 (*hprt1*) as housekeeping gene. Primers were tested for their efficiency beforehand, and the $\Delta\Delta C_t$-method was applied for analysis of relative expression. To ensure the specificity of the PCR product, we analyzed the melting curves of each product. Primer sequences were as follows (*gene*: forward primer, reverse primer); *Hprt1*: GATTAGCGATGATGAA CCAGGTT, CCTCCCATCTCCTTCATGACA; *P2ry6*: GCTGTGTCAGAGGG AGTTTT, TGTCAGCCTTTCCTATGCTCG; *P2ry12*: GCACGGACACTTTC CCGTAT, GCCTTGAGTGTTTCTGTAGGGTA; *Tlr2*: GACGACTGTACCCT CAATGG, TTAAATGCTGGGAGAACGAG; *Tlr4*: AGACCTCAGCTTCAAT GGTG, GAGACTGGTCAAGCCAAGAA; *Tlr7*: ATGTGGACACGGAAGAG ACAA, GGTAAGGGTAAGATTGGTGGTG.

2.11. Multiplex immune assay

Cytokine detection was performed using the mouse High Sensitivity 5−plex Multiplex Immunoassay (Thermofisher Scientific, Waltham, MA, USA) on microglial cell supernatants collected following stimulation with LPS (100 ng/ml), Pam2CSK4 (100 ng/ml) or Loxoribine (1 mM) for 24 h, according to the manufacturer's recommendations. This magnetic bead-based assay enables the simultaneous detection and quantification of multiple proteins in a single sample. Prior to incubation, samples were vortexed followed by centrifugation to remove

particles. Protein detection was performed on a multiplexing plate reader (Luminex 200, R&D Systems, Minneapolis, USA) and analyzed using Bioplex System Software 4.0 (Bio-Rad, Hercules, CA, USA). Cytokines analyzed included IL-6, TNF-α, IFN- γ, IL-2 and IL-4. Expression levels are shown as Fluorescent Intensity (FI).

2.12. cAMP ELISA

cAMP levels were determined using the cyclic AMP ELISA Kit (Biomol, Hamburg, Germany) according to the manufacturer's instructions. Briefly, MACS-isolated microglia were diluted in 50 µl HCl (0.1 M) and centrifuged for 10 min at 1000 *g*. Supernatant was diluted in 100 µl ELISA buffer to neutralize the acid. Sample acetylation was performed by adding 30 µl KOH (4 M) and 7.5 µl acetic anhydride, vortexing for 15 s and adding 7.5 µl KOH (4 M). Samples and standards were pipetted into the ELISA plates and incubated for 18 h at 4 °C before the plate was developed with Ellmann's reagent. Fluorescence was measured at 420 nm using a plate reader (Luminex 200, R&D Systems, Minneapolis, USA).

2.13. Cell viability assay

Cell viability was evaluated using the CellTiter-Glo® Luminescent Cell Viability Assay Kit (Promega, Walldorf, Germany) according to the manufacturer's instructions. Briefly, 2×10^4 MACS-isolated microglia (in 100 µl PBS) were seeded into each well of a 96 well plate, followed by the addition of 100 µl CellTiter Glo® reagent and vertical shaking for 10 min at 4 °C. Luminescence was determined using a luminescence plate reader (Luminex 200, R&D Systems, Minneapolis, USA) after a 30 min incubation at room temperature. Three animals were used for each condition (male and female WT and *Nf1*+/−), and three technical replicates were generated.

2.14. Statistics

All data are expressed as mean ± SEM. A combination of one-way ANOVA tests with Tukey post hoc tests were employed to compare data between the four experimental groups. Significance is always given as *** $p < .001$, ** $p < .01$, * $p < .05$, n.s. $p > .05$.

3. Results

3.1. Microglia density and morphology are not altered by sex or Nf1 mutation

To determine whether *Nf1* mutation or sex alters cellular and/or microglia content in the brain, we first determined the density of microglia in cortex, hippocampus (CA2–3 region), subgranular zone (SGZ) and amygdala from male and female *Nf1*+/− and WT mice. Using DAPI to detect the total number of cells, we found no differences in cellular densities with respect to sex or *Nf1* mutation (Suppl. Fig. 1 and Table 1). Similar results were obtained when the density of microglia was quantified. In addition, microglial morphology (ramified versus amoeboid appearance) was not different between groups.

3.2. Cytokine release following toll-like receptor stimulation is not different between microglia from male and female WT and Nf1+/− mice

Toll-like receptors (TLRs) are expressed on microglia, where they recognize pathogen-associated molecules, like bacterial and viral components. Upon activation, TLR signaling culminates with the production of inflammatory molecules. To characterize TLR responses, we generated microglial cultures from adult (12–16 weeks) male and female WT and *Nf1*+/− mice, and stimulated them for 24 h with LPS, LOX or Pam2CSK4 to activate TLR4-, TLR7- and TLR2-mediated pathways, respectively. The release of TNF-α, IL-6, IL-2, IL-4 and IFN-γ was then measured from the culture supernatants using a multiplex ELISA immunoassay. No differences between microglial cultures from male and female WT and *Nf1*+/− mice were detected (Suppl. Fig. 2), indicating that these inflammatory responses were not impacted by either sex or *Nf1* mutation. Consistent with these findings, no differences in microglial Tlr2, Tlr4 and Tlr7 expression were observed between male and female WT and *Nf1*+/− mice (Suppl. Fig. 4).

3.3. Phagocytic activity is reduced in Nf1+/− mice

Phagocytosis is an important function of microglia that enables them to control synaptic density and plasticity, as well as to maintain brain homeostasis under inflammatory conditions. To assay microglial phagocytic activity, we employed cortical slices from male and female *Nf1*+/− and WT mice between 14 and 16 weeks of age (Wendt et al., 2017). Phagocytic activity was quantified by incubating the slices for 60 min with latex beads, and counting the number of beads incorporated into a 3D-rendered Iba1-labeled (microglia) volume using confocal imaging and 3D reconstruction (Fig. 1 A). Per animal and condition, we quantified microglial phagocytosis in 4–5 cortical brain slices, analyzing 4–5 randomly chosen fields of view per slice by z-stacks (cortex layers I–VI; 5–6 female and 5–6 male WT and *Nf1*+/− mice each; 2–3 mice for AR-C66096 treatment, Fig. 1 A). As shown in Fig. 1 B, baseline microglial phagocytosis was not significantly different between female and male WT mice (male WT: 1.76 ± 0.12, $n = 69$ cells; female WT: 1.82 ± 0.13, $n = 83$ cells; $p = .7220$), consistent with a previous study from our laboratory (Guneykaya et al., 2018). In striking contrast, microglia from both male and female *Nf1*+/− mice displayed reduced phagocytic activity relative to WT mice (male *Nf1*+/−: 1.29 ± 0.09; $n = 78$ cells; $p = .0026$ vs male WT; female *Nf1*+/−: 1.43 ± 0.11; $n = 66$ cells; $p = .0209$ vs female WT), indicating an *Nf1*-dependent decrease in microglial phagocytosis.

Table 1
Cellular and microglial densities in different brain regions. (n = number of mice).

Brain region	M WT		M *Nf1*		F WT		F *Nf1*		*p* value (ANOVA)
	cells/mm²	*n*	*cells/mm²*	*n*	*cells/mm²*	*n*	*cells/mm²*	*n*	
Ctx	2773.2 ± 215.8	8	3207.8 ± 142.0	9	2913.4 ± 276.7	9	2895.0 ± 246.9	10	0.6005
HC	3075.9 ± 89.3	9	3129.5 ± 92.4	9	3063.9 ± 38.6	9	3178.0 ± 58.2	10	0.6574
SVZ	2917.1 ± 70.7	9	2973.9 ± 43.3	9	2754.3 ± 66.6	9	2855.4 ± 62.7	10	0.1007
Amy	3960.8 ± 182.4	8	3847.4 ± 110.1	8	3920.4 ± 86.3	8	4178.4 ± 108.5	8	0.4561
	microglia/mm²	***n***	***microglia/mm²***	***n***	***microglia/mm²***	***n***	***microglia/mm²***	***n***	
Ctx	250.3 ± 31.6	7	267.5 ± 26.2	9	179.5 ± 16.9	9	225.4 ± 30.3	9	0.5034
HC	199.8 ± 22.7	9	212.9 ± 20.7	9	147.2 ± 17.9	9	174.5 ± 33.5	10	0.2867
SVZ	169.1 ± 35.6	9	116.0 ± 12.8	9	103.9 ± 23.2	9	103.7 ± 23 7	10	0.2279
Amy	321.7 ± 20.8	6	321.6 ± 32.9	8	261.2 ± 22.5	2	297.8 ± 26.6	8	0.3514

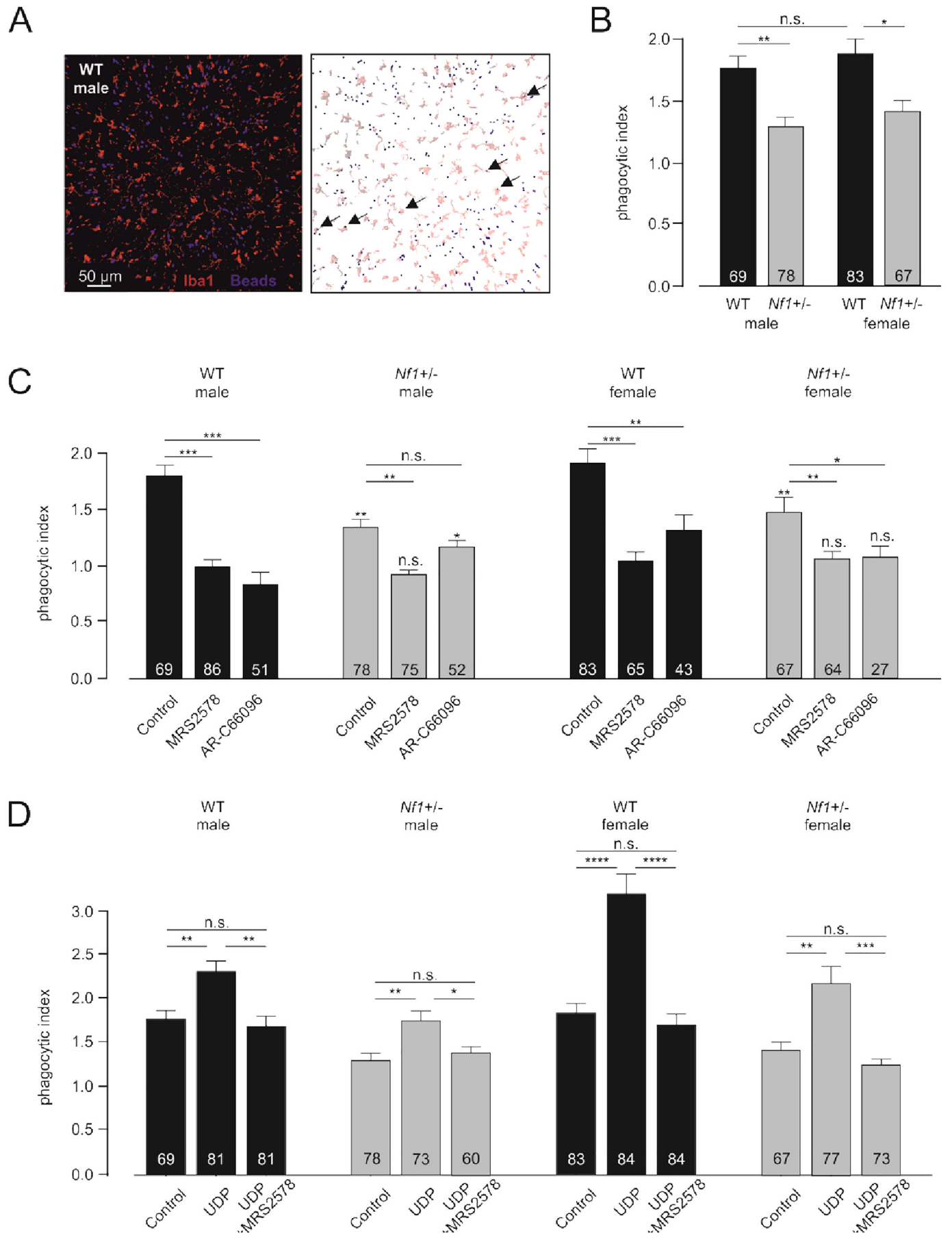

(caption on next page)

Fig. 1. Impaired phagocytic activity of microglia from *Nf1+/−* mice.
A: Representative confocal image (*left*) of Iba1-stained microglia (red) together with latex beads (blue) performed on brain slices from a representative 13-week-old WT male mice. Right, 3D reconstructions of Iba1-positive microglia are shown with automatically counted phagocytosed beads (shown in black and indicated by arrows). Scale bars, 50 μm.
B: Comparison of baseline phagocytic index of cortical microglia reveals lower levels in male and female *Nf1+/−* mice.
C: Control of microglial baseline phagocytosis by the P2ry6 and P2ry12 purinergic receptors. Blockade of P2ry6 by MRS2578 (5 μM) reduced baseline phagocytosis in all four groups (male and female WT and *Nf1+/−* mice). Blockade of P2ry12 by AR-C66096 (1 μM) decreased microglial baseline phagocytosis only in male WT, female WT, and female *Nf1+/−* mice, but not in male *Nf1+/−* mice.
D: P2ry6-mediated stimulation of microglial phagocytosis is dependent on sex or *Nf1* mutation. Phagocytosis in the presence of the P2ry6 agonist UDP (100 μM), the P2ry6 antagonist MRS2578 (5 μM), and UDP + MRS2578 are indicated. UDP-mediated stimulation of phagocytosis in all groups (male and female WT and *Nf1+/−* mice) was blocked by MRS2578, indicating that P2ry6 signaling is unaffected by sex or *Nf1* mutation.
The significance levels above the bars indicate the comparisons between WT and *Nf1+/−* mice; *** $p < .001$, ** $p < .01$, * $p < .05$, n.s. $p > .05$. Numbers in the bars indicate the number of analyzed viewfields. Data were obtained from 3 to 9 mice and 12–36 slices per condition. (For interpretation of the references to colour in this figure legend, the reader is referred to the web version of this article.)

3.4. Purinergic signaling alters microglial phagocytic activity in a sex- and Nf1-dependent manner

It is well established that purinergic signaling controls microglial phagocytosis, specifically through the purinergic receptors, P2RY6 (Koizumi et al., 2007; Xu et al., 2016; Wendt et al., 2017) and P2RY12 (Diaz-Aparicio et al., 2020). To examine the effect of purinergic signaling on basal phagocytic activity in *Nf1*-mutant microglia, we evaluated P2RY6 and P2RY12 receptor signaling using receptor-specific inhibitors (MRS2578, 5 μM and AR-C66096, 1 μM, respectively) (Fig. 1 C). MRS2578 reduced the phagocytic activity of microglia to a similar level in all groups, male and female WT and *Nf1+/−*, suggesting that *Nf1*-dependent reduction in basal phagocytosis of both sexes (Fig. 1 B) is likely due to P2RY6-dependent mechanisms. However, treatment with the P2RY6 ligand UDP (100 μM), enhanced phagocytosis in all of the four groups (Fig. 1 D, Table 2) indicating that there was no general failure in P2RY6 signaling in male and female *Nf1+/−* microglia. This conclusion is also supported by our finding that there were no differences in *P2ry6* mRNA levels between male and female WT and *Nf1+/−* microglia (Suppl. Fig. 4).

P2RY12 inhibition reduced microglial phagocytosis similar to that observed following P2RY6 blockade in male and female WT mice (Fig. 1 C, Table 2). Relative phagocytic activities in the presence of AR-C66096 were 0.80 ± 0.10 for male WT microglia ($p < .001$ vs. control and $p = .1676$ vs. MRS2578) and 1.26 ± 0.16 for female WT microglia ($p < .001$ vs. control and $p = .1635$ vs. MRS2578). Interestingly, AR-C66096 did not decrease basal microglial phagocytosis in *Nf1+/−* male mice (1.12 ± 0.11, $n = 52$; $p = .2256$ vs male *Nf1+/−* control), indicating a reduced contribution of P2RY12 signaling to baseline phagocytic activity. In female *Nf1+/−* mice, AR-C66096 reduced microglial phagocytic activity similar to female WT mice (1.03 ± 0.14, $n = 27$; $p = .0291$ vs female *Nf1+/−* control). Taken together, the P2RY12-mediated microglia phagocytosis is altered in a sexually dimorphic fashion in the setting of a heterozygous *Nf1* mutation.

3.5. P2RY-dependent microglia membrane currents are impaired in male Nf1+/− mice

Microglia express a variety of purinergic receptors, including members of the metabotropic P2Y and ionotropic P2X receptor families. We have previously shown that microglial membrane current responses upon application of low (10 μM) ATP concentrations largely depend on P2RY12 activation (Elmadany et al., 2020), which activates K^+ currents through THIK-1 (Wendt et al., 2017; Boucsein et al., 2000; Boucsein et al., 2003; Madry et al., 2018; Guneykaya et al., 2018). We analyzed purinergic P2RY12 responses of microglia in acute cortical slices from 14 to 16 week old male and female *Nf1+/−* mice using standard whole-cell patch clamp techniques in the voltage-clamp configuration. The microglial cells in each slice were identified by fluorescence labeling in WT and *Nf1+/−* mice intercrossed with MacGreen (Csf1r-GFP) mice. Consistent with previous studies, WT microglia responded to 10 μM ATP with the induction of an outwardly rectifying current that reversed close to the equilibrium potential for potassium. We determined the specific conductance between +20 mV and +60 mV to compare these currents in male and female microglia. The conductance of microglial ATP-evoked potassium currents was 27.0 ± 4.6 pS/pF and 25.4 ± 5.2 pS/pF for male and female WT microglia, respectively ($n = 21$ and $n = 19$ cells, respectively; $p = .8201$, Fig. 2 A, B). Similar to the microglia phagocytosis results, these microglial purinergic responses were reduced in male *Nf1+/−* mice (15.7 ± 2.5 pS/pF; $n = 36$ cells; $p = .0234$ vs. male WT), indicating an *Nf1*-dependent impairment. In contrast, 10 μM ATP responses of female *Nf1+/−* microglia (23.3 ± 5.9 pS/pF; $n = 16$ cells; $p = .9671$) were not different from WT females, indicating a sexually dimorphic impairment of P2RY12 signaling in the setting of an *Nf1* mutation.

3.6. P2X-dependent purinergic membrane currents are not altered in Nf1+/− mice

To analyze P2X receptor signaling, we measured microglial membrane currents evoked by the application of 1 mM ATP (Fig. 2 C, D), a concentration sufficient to activate P2RX7, the most common P2X receptor isoform in microglia (Butovsky et al., 2014; Ousingsawat et al., 2015). 1 mM ATP application induced large membrane currents within the application period (60 s), which were characterized by an inward and outward component and a reversal potential close to 0 mV, consistent with the characteristics of the non-selective cation channel

Table 2
Purinergic receptors regulate microglia phagocytosis.

Condition	♂ WT		♂ *Nf1*		♀ WT		♀ *Nf1*	
	*engulfed beads*10³/μm³*	*n*	*engulfed beads*10³/μm³*	*n*	*engulfed beads*10³/μm³*	*n*	*engulfed beads*10³/μm³*	*n*
control	1,76 ± 0,12	69	1,29 ± 0,09	78	1,82 ± 1,13	83	1,43 ± 0,11	66
UDP	2,30 ± 0,14	81	1,74 ± 0,12	73	3,18 ± 0,22	84	2,17 ± 0,22	77
UDP & MRS2578	1,68 ± 0,13	81	1,38 ± 0,09	60	1,69 ± 0,14	84	1,24 ± 0,08	73
MRS2578	0,99 ± 0,10	86	0,98 ± 0,08	75	1,00 ± 0,09	65	1,02 ± 0,08	64
AR-C66096	0,80 ± 0,10	51	1,12 ± 0,11	52	1,26 ± 0,16	43	1,03 ± 0,14	27

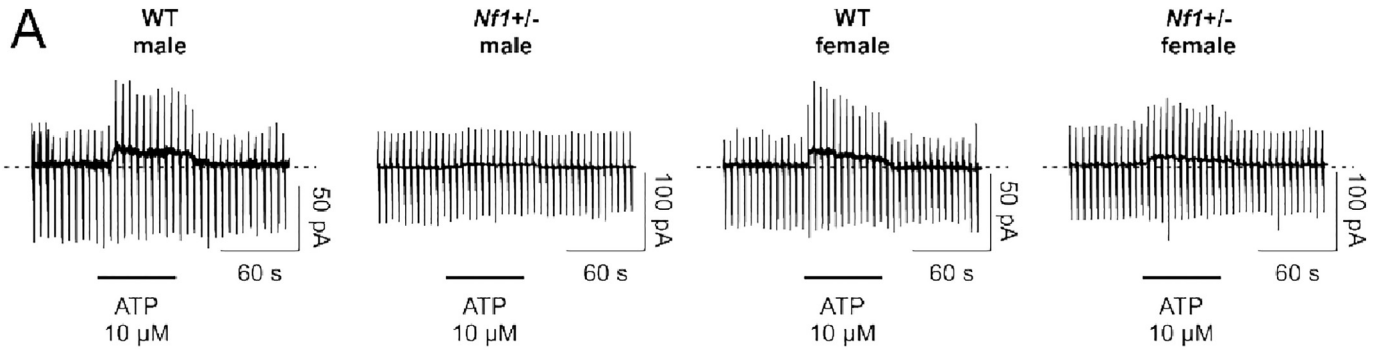

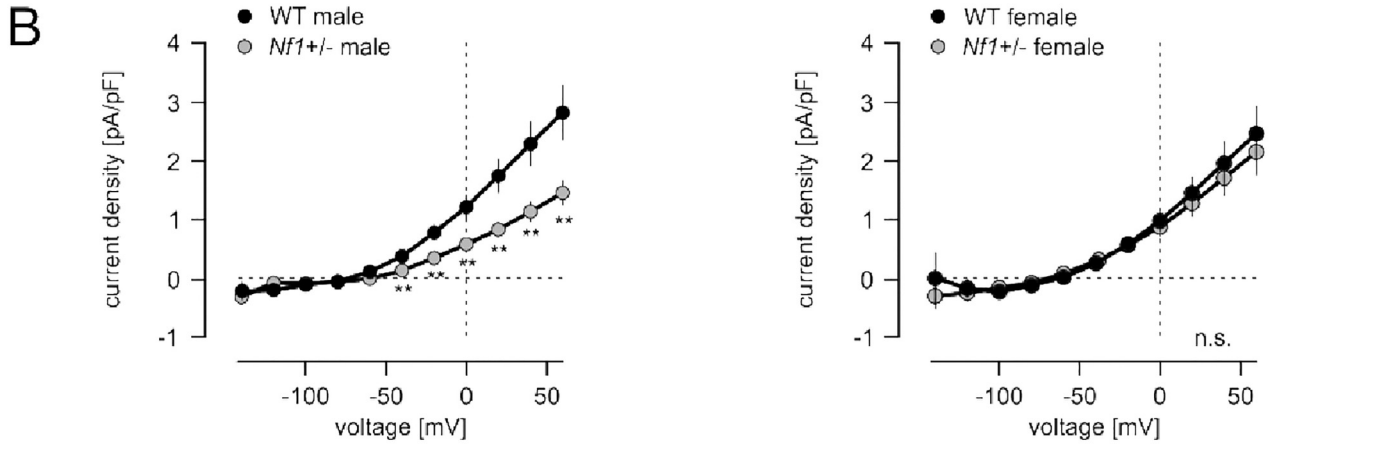

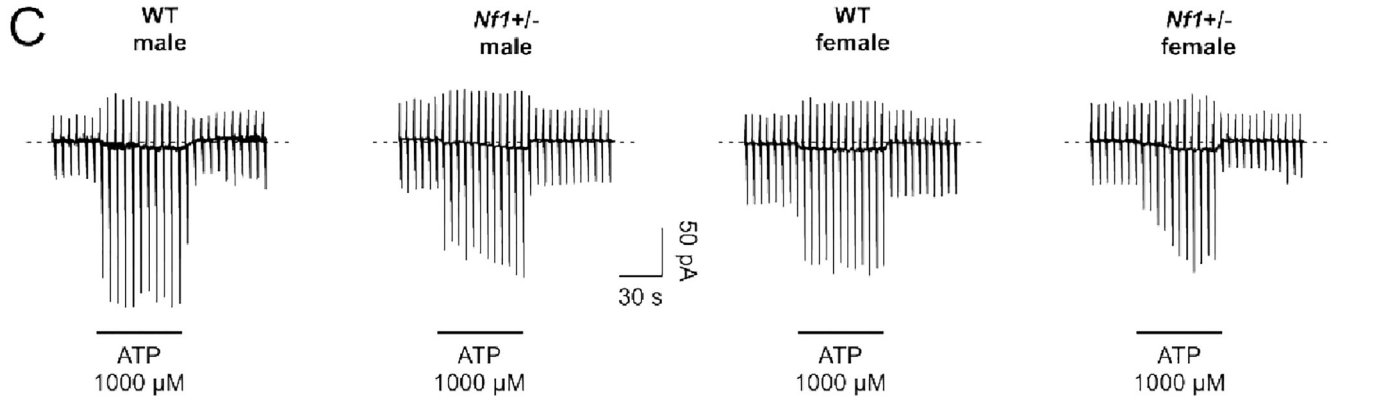

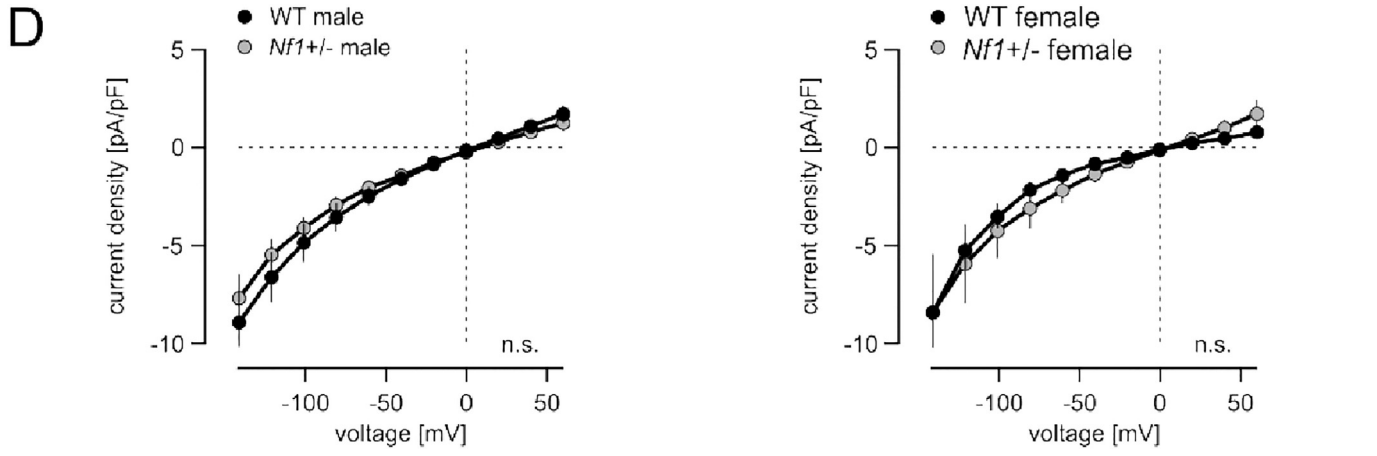

(caption on next page)

Fig. 2. *Nf1*-dependent alterations in microglial purinergic membrane current responses.
A and C: Representative patch-clamp recordings from male and female WT and *Nf1* +/− microglia. From a holding potential of −20 mV, cells were repetitively clamped at a series of potentials between −140 and +60 mV every 5 s. Application of 10 μM ATP (A) or 1000 μM ATP (C) is indicated by the bars. Note the typical metabotropic purinergic response to 10 μM ATP with activation of outwardly rectifying currents (A) and the typical P2X-like induction of a cationic conductance upon 1000 μM ATP (C) exposure.
B and D: Averaged current density-voltage relationships of currents evoked by 10 μM ATP (B) or 1000 μM ATP (D). Current responses were obtained by subtraction of microglial membrane currents prior to and in the presence of 10 μM (B) or 1000 μM (D) ATP, followed by normalization to the capacitance.
Male *Nf1* +/− mice displayed significantly smaller metabotropic purinergic responses (ANOVA/Tukey). Number of recorded cells (mice): male WT, 26 (12); male *Nf1* +/−, 29 (14); female WT, 19 (11); female *Nf1* +/−, 16 (10).
There were no significant sex- or *Nf1*-dependent differences in P2X-like currents (ANOVA/Tukey).
Number of recorded cells (mice): male WT, 13 (9); male *Nf1* +/−, 14 (11); female WT, 7 (6); female *Nf1* +/−, 12 (9).

(Fig. 2 C). The specific conductance between −100 mV and − 140 mV was quantified to compare P2X-like currents in male and female WT microglia. Conductances were 102.1 ± 18.2 pS/pF (n = 13 cells) and 122.8 ± 44.1 pS/pF (n = 7 cells) for male and female WT microglia, respectively (p = .6150). P2X receptor-like currents in cortical microglia from male and female *Nf1* +/− mice were similar to their WT counterparts (89.9 ± 21.0 pS/pF; n = 14 cells; p = .6678 for male and 114.7 ± 36.4 pS/pF; n = 12 cells; p = .8920 for female), demonstrating that the *Nf1* mutational and sexually dimorphic differences in microglia purinergic signaling were specific to metabotropic P2Y receptor signaling.

3.7. Basic membrane properties of microglia are not Nf1-dependent

Consistent with previous data from our laboratory and others (see Kettenmann et al., 2011), microglia from 14 to 16 week old WT mice display characteristic membrane currents when repetitively clamped at potentials between −170 and +60 mV, starting from a holding potential of −70 mV. Microglia are characterized by a high input resistance and a small inwardly rectifying conductance between −40 and − 170 mV (Suppl. Fig. 3 A, B). The reversal potential, indicative of the resting membrane potential, was −27.7 ± 1.2 mV (n = 27 cells) and − 29.2 ± 2.2 mV (n = 23 cells) for male and female WT microglia, respectively (p = .5435), as previously described (Guneykaya et al., 2018). The apparent membrane capacitance was not different between the two sexes, with microglia from male WT mice having 21.0 ± 1.2 pF (n = 27 cells) and from female WT mice 23.2 ± 1.3 pF (n = 11 cells; p = .2272; Suppl. Fig. 3 C, D). However, in contrast to our previous study (Guneykaya et al., 2018), the amplitude of the inwardly rectifying currents were not significantly different between male and female WT microglia (p = .2508). This could be potentially explained by differences in the mouse strains used in these two studies. Additionally, cortical microglia from *Nf1* +/− mice did not differ from their WT counterparts with respect to reversal potentials (male *Nf1* +/−: n = 47 cells; p = .1589 vs WT; female *Nf1* +/−: n = 37 cells; p = .3385 vs WT) and capacitance (male: p = .9342; female: p = .3553). Inwardly rectifying currents were also not different between male (p = .0681) or female (p = .0754). WT and *Nf1* +/− microglia. Taken together, there are no sex-dependent differences in the electrophysiological profiles of cortical microglia in normal mice or in the setting of an *Nf1* mutation.

3.8. Microglial process extension is impaired in male Nf1 +/− mice

Another P2RY12-mediated function in microglia is process extension in response to injury (Haynes et al., 2006; Madry et al., 2018; Guneykaya et al., 2018), where microglia respond with targeted movement of their processes towards the lesion site (Nimmerjahn et al., 2005; Davalos et al., 2005). Microglial responses in acute brain slices of adult (13–15 weeks) male and female WT and *Nf1* +/− mice on a MacGreen background were analyzed following a laser lesion by two-photon imaging. The movement of microglial processes was quantified by determining the fluorescence distribution within the area of concentric circles (45 μm and 90 μm) around the lesion site (for details, see Materials and Methods; Fig. 3 A). The response of male WT microglia 30 min after the laser lesion was 0.043 ± 0.004 (n = 21 cells), which was greater than observed in female WT microglia (0.027 ± 0.002; n = 26 cells; p = .0014). No translocation of microglial cell bodies was seen during the observation period. In contrast, whereas female *Nf1* +/− microglia exhibited no differences (0.021 ± 0.003; n = 20 cells; p = .4798) relative to their WT counterparts, process extension in male *Nf1* +/− microglia was decreased to 0.015 ± 0.002 (n = 20 cells; p < .0001) relative to male WT controls.

3.9. Microglial cAMP levels are reduced in male Nf1 +/− mice

To determine the basis for the sexual dimorphism in microglia purinergic signaling observed in male *Nf1* +/− mice, we first examined P2RY6 and P2RY12 mRNA expression in acutely isolated microglia from adult mouse brains (14–16 weeks). Following MACS (CD11b) isolation, qPCR using P2RY6- and P2RY12-specific primers (Suppl. Fig. 4) revealed no differences in mRNA expression between male and female WT and *Nf1* +/− microglia, excluding receptor expression levels as the causative etiology for the differences in purinergic signaling.

Next, we examined intracellular cAMP levels, based on prior studies in astrocytes (Dasgupta et al., 2003; Anastasaki and Gutmann, 2014) and the fact that purinergic signaling results in increased cAMP generation (Post et al., 1996; Post et al., 1998). Microglia were isolated from whole brains of male and female WT and *Nf1* +/− mice (12–16 weeks) by MACS using CD11b antibodies, and subjected to ELISA to measure intracellular cAMP levels (Fig. 4 A). We first performed a cell viability assay on MACS-isolated microglia from the four groups and excluded potential sex- or genotype-dependent differences in microglial persistence to the MACS isolation procedure (Suppl. Fig. 5). cAMP levels were similar in female (1.8 ± 0.3 pg/ml, n = 3 mice) and male (2.5 ± 0.1 pg/ml; n = 3 mice; p = .1772) WT microglia, however, reduced microglial cAMP levels were observed in male *Nf1* +/− (1.4 ± 0.3 pg/ml, n = 3 mice) relative to WT (p = .0301) microglia (Fig. 4 B). In contrast, female *Nf1* +/− microglia (1.7 ± 0.1 pg/ml, n = 3 mice) did not differ from WT controls (p = .9950), indicating that microglial cAMP levels are affected by *Nf1* mutation in a sexually-dimorphic manner.

3.10. Increasing intracellular cAMP levels rescues male Nf1 +/− microglia phenotypes

To restore intracellular cAMP levels in microglia, we took advantage of the preferential expression of the phosphodiesterase (PDE) 3B subtype in microglia, and used cilostamide, a selective PDE3 inhibitor, to increase cAMP levels in microglia in situ (Bernier et al., 2019). Treatment with 10 μM cilostamide for 10 min resulted in a normalization of ATP-(10 μM) induced outward currents in microglia from male *Nf1* +/− mice similar to levels observed in WT male microglia (Fig. 4 C, D). In addition, cilostamide treatment also ameliorated the male *Nf1* +/− microglia defect in directed process movement towards a laser lesion. Pretreatment of slices with 10 μM cilostamide for 10 min partly corrected the movement defect in male *Nf1* +/− microglia (Fig. 4 E, F). Taken together, these data establish that the sexually dimorphic *Nf1* +/

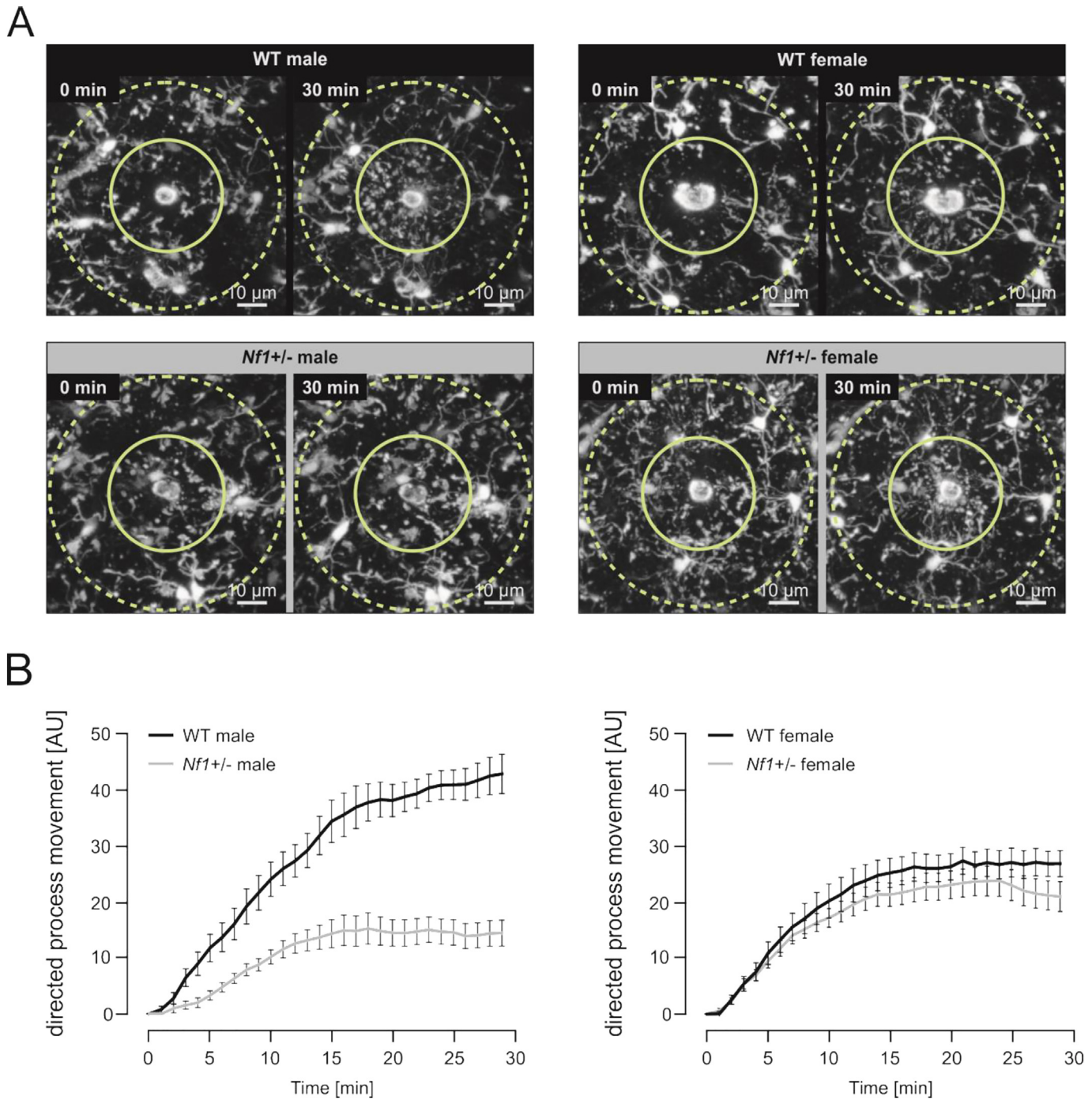

Fig. 3. Injury-directed process movement activity is decreased in male *Nf1*+/− microglia.
A: Representative pictures of injury-induced process movement of EGFP-positive microglia in the cortex of acute brain slices from male and female WT and *Nf1*+/− mice. Acute injury was induced by a focal laser lesion (left images) and microglial movement activity was recorded for 30 min (right images). Yellow lines indicate the concentric circles (solid: 45 µm; dotted: 90 µm) around the lesion site used for offline quantification of microglial process movements.
B: Quantitative analysis of lesion-induced, microglial process movement expressed in arbitrary units (AU) in male and female WT and *Nf1*+/− mice. (For interpretation of the references to colour in this figure legend, the reader is referred to the web version of this article.)
Male *Nf1*+/− microglia displayed significantly weaker process responses than male WT microglia. Number of experiments (and mice): male WT, 21 (9); male *Nf1*+/−, 20 (6); female WT, 26 (9); female *Nf1*+/−, 20 (6).

− microglia purinergic signaling defects result from alterations in intracellular cAMP levels.

4. Discussion

In this report, we demonstrate that sex and genotype interact to result in male-specific defects in microglial purinergic signaling, leading to impaired phagocytosis, process movement, and membrane currents. These observations fortify prior observations that male microglia contribute differentially to brain pathology. For example, P2RX4 is uniquely induced in male microglia after injury (Sorge et al., 2015), resulting in male pain hypersensitivity. Similarly, male, but not female, microglia exhibit ATP-dependent p38-MAPK phosphorylation and brain-derived neurotrophic factor (BDNF) release (Mapplebeck

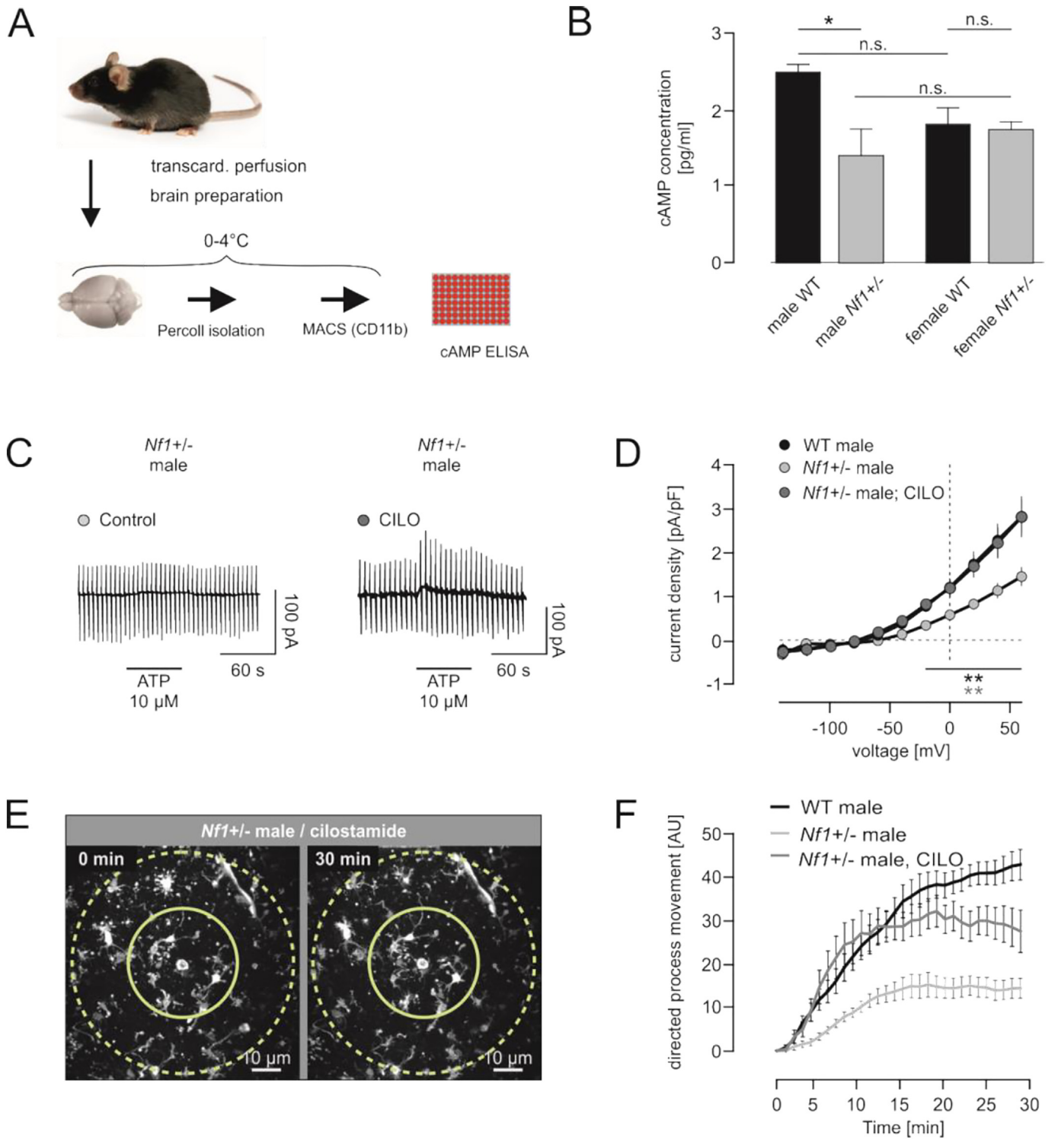

(caption on next page)

et al., 2018). While these sex differences could reflect the differential expression of purinergic receptors (e.g., P2RX4, P2RX7, P2RY12) in male microglia (Guneykaya et al., 2018), this was not the etiology for the sex-by-genotype effects observed in male *Nf1*-mutant microglia. Instead, we discovered that cAMP differences in male *Nf1+/−* microglia underlie these sexually dimorphic phenotypes in young adult mice (12–16 weeks of age). As age affects microglial function and sex differences throughout lifespan, these sex by genotype effects might be different in older or younger mice.

The role of cAMP in microglia ramification and process movement has previously been shown using PDE inhibitors and G protein-coupled receptor activation (Bernier et al., 2019). In addition, norepinephrine-dependent changes in microglial morphology and function in awake and anesthetized mice are cAMP dependent (Stowell et al., 2019; Liu et al., 2019). In the setting of *Nf1* mutation, the *Nf1* protein (neurofibromin) controls cAMP homeostasis in human and mouse neurons through RAS-mediated activation of an atypical Protein Kinase-C (PKCζ), resulting in reduced G protein-coupled receptor stimulation of

Fig. 4. Decreased cAMP levels in male *Nf1* +/− microglia determine their functional impairments.
A and B: Intracellular cAMP levels are decreased in male *Nf1* +/− microglia. A, Scheme representing the procedure for determining microglial cAMP levels in male and female WT and *Nf1* +/− mice. Microglia were MACS-isolated (CD11b) from whole brains in the cold (0–4 °C), and then prepared for commercial ELISA (see methods). B, While there were significant differences in cAMP levels between male WT and *Nf1* +/− microglia, no differences were observed between female WT and *Nf1* +/− microglia.
C and D: Cilostamide restores impairments in P2RY12-dependent membrane responses. C, Representative patch-clamp recordings from male *Nf1* +/− microglia. From a holding potential of −20 mV, cells were repetitively clamped at a series of potentials between −140 and + 60 mV every 5 s. Application of 10 μM ATP is indicated by the bars. Note that the decrease in typical metabotropic purinergic responses upon 10 μM ATP with an activation of outwardly rectifying currents was restored by cilostamide (10 μM) treatment. D, Averaged current density-voltage relationships of currents evoked by 10 μM ATP in the presence or absence of cilostamide. Current responses were obtained by subtraction of microglial membrane currents prior to and in the presence of 10 μM ATP and subsequent normalization to the capacitance.
E and F: Impaired directed process movement in male *Nf1* +/− microglia is restored by cilostamide treatment. E, Representative images of injury-induced process movement of EGFP-positive microglia in the cortex of acute brain slices from male *Nf1* +/− mice in the presence of 10 μM cilostamide. Acute injury was induced by a focal laser lesion (left images), and microglial responses were observed for 30 min (right images). Yellow lines indicate the concentric circles (normal: 45 μm; dotted: 90 μm) around each lesion site used for offline quantification of microglial process movements. F, Quantitative analysis of lesion-induced, microglia process movement in male WT and *Nf1* +/− mice. Note the rescue of process movement in male *Nf1* +/− microglia following cilostamide treatment; one-way ANOVA and Tukey tests were performed. $N = 9$ experiments (4 mice) for cilostamide-treated slices. (For interpretation of the references to colour in this figure legend, the reader is referred to the web version of this article.)

adenylyl cyclase (Anastasaki and Gutmann, 2014). However, it is not known how neurofibromin regulates cAMP homeostasis in microglia or whether the observed sexual dimorphic effects involve gonadal sex hormone or sex chromosome differences (Arnold, 2009), microbiome influences (Thion et al., 2018) or the differential expression of regulatory microRNAs (Kodama et al., 2020).

In patients with NF1, impulsivity and hyperactivity is more common in boys than girls (Cohen et al., 2018), and, as seen in the general population, there is a male bias in the prevalence of autism spectrum disorders (ASD) in children with NF1 (Garg et al., 2016). In this regard, previous studies from our laboratory demonstrated that male, but not in female, *Nf1* +/− mice exhibit reduced hippocampal dopamine levels, increased RAS/ERK activity, and impaired spatial learning (Diggs-Andrews et al., 2014b). In the current study, we investigated microglial cells, which are, particularly during early postnatal stages, critical for the development and homeostasis of neuronal networks, mainly due to their ability to prune synapses (Tremblay et al., 2011; Kettenmann et al., 2013; Bilimoria and Stevens, 2015; Michell-Robinson et al., 2015). As such, there is growing evidence for a crucial role of microglia in the development psychiatric disorders including schizophrenia (Mattei et al., 2014) and ASD (Petrelli et al., 2016). Since no direct evidence exists for such a causal link in the setting of NF1, future studies will be required to elucidate the impact of reduced microglial P2RY12 activity on social interaction phenotypes in male and female *Nf1*-mutant mice.

Taken together, the finding of sexually dimorphic differences in microglia harboring a germline *Nf1* mutation adds to the growing number of sex-specific abnormalities described in microglia, including differences in morphology (Lenz et al., 2013), function (Nelson et al., 2017), and density (Schwarz et al., 2012; Vanryzin et al., 2019). In addition, male and female microglia also have different rates of transcriptional maturation and immune reactivity (Hanamsagar et al., 2017; Guneykaya et al., 2018). Some of these differences may be “hard wired” by sex, given that female microglia offer protection in the face of ischemic injury when transplanted into male brains (Villa et al., 2018). Understanding how these sex differences are established and maintained will provide new insights into our understanding of the interplay between risk factors and cellular function in the brain.

Acknowledgements

We thank Regina Piske and Nadine Scharek, for their excellent technical assistance. The work was supported by the NeuroCure Cluster of Excellence grant to H.K., a National Cancer Institute grant (1-R01-CA214146-01 to D.H.G.) and a Berlin Institute of Health/ Einstein fellowship grant to D.H.G. and H.K. D.H.G. is an Alexander von Humboldt Fellow. N.E. is a DAAD scholar. This work was also supported by services provided by the Advanced Light Microscopy facility (MDC, Berlin).

Author contributions

N.E., A.S. and M.S. performed the electrophysiology experiments; N.E., F.L. and R.P. performed the phagocytosis experiment; V.H. performed the qRT-PCR experiments; F.L. performed the laser lesion experiments; A.B. performed density and multiplex ELISA experiments. E.L.W.-J. performed additional experiments during the execution of this project, N.E., E.C.W.-J. and M.S. wrote the first draft of the manuscript and prepared the figures; N.E. and M.S. supervised the trainees (R.P. and A.S.) who participated in performing the experiments; M.S., H.K., and D.H.G. designed the experiments; H.K. and D.H.G. oversaw the studies, mentored the trainees, revised the manuscript and provided funding for this project.

Data availability section

No protein or modeling script datasets were produced in this study.

Declaration of Competing Interest

The authors declare no relevant conflicts of interest.

Appendix A. Supplementary data

Supplementary data to this article can be found online at https://doi.org/10.1016/j.nbd.2020.105030.

References

Anastasaki, C., Gutmann, D.H., 2014. Neuronal NF1/RAS regulation of cyclic AMP requires atypical PKC activation. Hum. Mol. Genet. 23, 6712–6721.
Arnold, A.P., 2009. The organizational-activational hypothesis as the foundation for a unified theory of sexual differentiation of all mammalian tissues. Horm. Behav. 55, 570–578.
Bennett, M.L., Bennett, F.C., 2020. The influence of environment and origin on brain resident macrophages and implications for therapy. Nat. Neurosci. 23, 157–166.
Bernier, L.P., Bohlen, C.J., York, E.M., Choi, H.B., Kamyabi, A., Dissing-Olesen, L., Hefendehl, J.K., Collins, H.Y., Stevens, B., Barres, B.A., Macvicar, B.A., 2019. Nanoscale surveillance of the brain by microglia via cAMP-regulated Filopodia. Cell Rep. 27, 2895–2908.e4.
Bilimoria, P.M., Stevens, B., 2015. Microglia function during brain development: new insights from animal models. Brain Res. 1617, 7–17.
Bloomfield, P.S., Bonsall, D., Wells, L., Dormann, D., Howes, O., De Paola, V., 2018. The effects of haloperidol on microglial morphology and translocator protein levels: an in vivo study in rats using an automated cell evaluation pipeline. J. Psychopharmacol. 32, 1264–1272.
Boucsein, C., Kettenmann, H., Nolte, C., 2000. Electrophysiological properties of microglial cells in normal and pathologic rat brain slices. Eur. J. Neurosci. 12, 2049–2058.
Boucsein, C., Zacharias, R., Farber, K., Pavlovic, S., Hanisch, U.K., Kettenmann, H., 2003.

Purinergic receptors on microglial cells: functional expression in acute brain slices and modulation of microglial activation in vitro. Eur. J. Neurosci. 17, 2267–2276.
Brannan, C.I., Perkins, A.S., Vogel, K.S., Ratner, N., Nordlund, M.L., Reid, S.W., Buchberg, A.M., Jenkins, N.A., Parada, L.F., Copeland, N.G., 1994. Targeted disruption of the neurofibromatosis type-1 gene leads to developmental abnormalities in heart and various neural crest-derived tissues. Genes Dev. 8, 1019–1029.
Butovsky, O., Jedrychowski, M.P., Moore, C.S., Cialic, R., Lanser, A.J., Gabriely, G., Koeglsperger, T., Dake, B., Wu, P.M., Doykan, C.E., Fanek, Z., Liu, L., Chen, Z., Rothstein, J.D., Ransohoff, R.M., Gygi, S.P., Antel, J.P., Weiner, H.L., 2014. Identification of a unique TGF-beta-dependent molecular and functional signature in microglia. Nat. Neurosci. 17, 131–143.
Cohen, R., Halevy, A., Aharon, S., Shuper, A., 2018. Attention deficit hyperactivity disorder in Neurofibromatosis type 1: evaluation with a continuous performance test. J. Clin. Neurol. 14, 153–157.
Dasgupta, B., Dugan, L.L., Gutmann, D.H., 2003. The neurofibromatosis 1 gene product neurofibromin regulates pituitary adenylate cyclase-activating polypeptide-mediated signaling in astrocytes. J. Neurosci. 23, 8949–8954.
Davalos, D., Grutzendler, J., Yang, G., Kim, J.V., Zuo, Y., Jung, S., Littman, D.R., Dustin, M.L., Gan, W.B., 2005. ATP mediates rapid microglial response to local brain injury in vivo. Nat. Neurosci. 8, 752–758.
Diaz-Aparicio, I., Paris, I., Sierra-Torre, V., Plaza-Zabala, A., Rodriguez-Iglesias, N., Marquez-Ropero, M., Beccari, S., Huguet, P., Abiega, O., Alberdi, E., Matute, C., Bernales, I., Schulz, A., Otrokocsi, L., Sperlagh, B., Happonen, K.E., Lemke, G., Maletic-Savatic, M., Valero, J., Sierra, A., 2020. Microglia actively remodel adult hippocampal neurogenesis through the phagocytosis Secretome. J. Neurosci. 40, 1453–1482.
Diggs-Andrews, K.A., Brown, J.A., Gianino, S.M., D'agostino Mcgowan, L., Rubin, J.B., Wozniak, D.F., Gutmann, D.H., 2014a. Reply: to PMID 24375753. Ann. Neurol. 75, 800–801.
Diggs-Andrews, K.A., Brown, J.A., Gianino, S.M., Rubin, J.B., Wozniak, D.F., Gutmann, D.H., 2014b. Sex is a major determinant of neuronal dysfunction in neurofibromatosis type 1. Ann. Neurol. 75, 309–316.
Elmadany, N., De Almeida Sassi, F., Wendt, S., Logiacco, F., Visser, J., Haage, V., Hambardzumyan, D., Wolf, S., Kettenmann, H., Semtner, M., 2020. The VGF-derived peptide TLQP21 impairs purinergic control of chemotaxis and phagocytosis in mouse microglia. J. Neurosci. 40 (17), 3320–3331.
Fisher, D.W., Bennett, D.A., Dong, H., 2018. Sexual dimorphism in predisposition to Alzheimer's disease. Neurobiol. Aging 70, 308–324.
Garg, S., Heuvelman, H., Huson, S., Tobin, H., Green, J., 2016. Sex bias in autism spectrum disorder in neurofibromatosis type 1. J. Neurodev. Disord. 8, 26.
Guneykaya, D., Ivanov, A., Hernandez, D.P., Haage, V., Wojtas, B., Meyer, N., Maricos, M., Jordan, P., Buonfiglioli, A., Gielniewski, B., Ochocka, N., Comert, C., Friedrich, C., Artiles, L.S., Kaminska, B., Mertins, P., Beule, D., Kettenmann, H., Wolf, S.A., 2018. Transcriptional and translational differences of microglia from male and female brains. Cell Rep. 24, 2773–2783.e6.
Gutmann, D.H., Ferner, R.E., Listernick, R.H., Korf, B.R., Wolters, P.L., Johnson, K.J., 2017. Neurofibromatosis type 1. Nat. Rev. Dis. Prim. 3, 17004.
Hanamsagar, R., Alter, M.D., Block, C.S., Sullivan, H., Bolton, J.L., Bilbo, S.D., 2017. Generation of a microglial developmental index in mice and in humans reveals a sex difference in maturation and immune reactivity. Glia 65, 1504–1520.
Haynes, S.E., Hollopeter, G., Yang, G., Kurpius, D., Dailey, M.E., Gan, W.B., Julius, D., 2006. The P2Y12 receptor regulates microglial activation by extracellular nucleotides. Nat. Neurosci. 9, 1512–1519.
Kerr, N., Dietrich, D.W., Bramlett, H.M., RAVAL, A.P., 2019. Sexually dimorphic microglia and ischemic stroke. CNS Neurosci. Ther. 25, 1308–1317.
Kettenmann, H., Hanisch, U.K., Noda, M., Verkhratsky, A., 2011. Physiology of microglia. Physiol. Rev. 91, 461–553.
Kettenmann, H., Kirchhoff, F., Verkhratsky, A., 2013. Microglia: new roles for the synaptic stripper. Neuron 77, 10–18.
Kodama, L., Guzman, E., Etchegaray, J.I., Li, Y., Sayed, F.A., Zhou, L., Zhou, Y., Zhan, L., Le, D., Udeochu, J.C., Clelland, C.D., Cheng, Z., Yu, G., Li, Q., Kosik, K.S., Gan, L., 2020. Microglial microRNAs mediate sex-specific responses to tau pathology. Nat. Neurosci. 23, 167–171.
Koizumi, S., Shigemoto-Mogami, Y., Nasu-Tada, K., Shinozaki, Y., Ohsawa, K., Tsuda, M., Joshi, B.V., Jacobson, K.A., Kohsaka, S., Inoue, K., 2007. UDP acting at P2Y6 receptors is a mediator of microglial phagocytosis. Nature 446, 1091–1095.
Krasemann, S., Madore, C., Cialic, R., Baufeld, C., Calcagno, N., El Fatimy, R., Beckers, L., O'loughlin, E., Xu, Y., Fanek, Z., Greco, D.J., Smith, S.T., Tweet, G., Humulock, Z., Zrzavy, T., Conde-Sanroman, P., Gacias, M., Weng, Z., Chen, H., Tjon, E., Mazaheri, F., Hartmann, K., Madi, A., Ulrich, J.D., Glatzel, M., Worthmann, A., Heeren, J., Budnik, B., Lemere, C., Ikezu, T., Heppner, F.L., Litvak, V., Holtzman, D.M., Lassmann, H., Weiner, H.L., Ochando, J., Haass, C., Butovsky, O., 2017. The TREM2-APOE pathway drives the transcriptional phenotype of dysfunctional microglia in neurodegenerative diseases. Immunity 47, 566–581.e9.
Lenz, K.M., Nugent, B.M., Haliyur, R., Mccarthy, M.M., 2013. Microglia are essential to masculinization of brain and behavior. J. Neurosci. 33, 2761–2772.
Liu, Y.U., Ying, Y., Li, Y., Eyo, U.B., Chen, T., Zheng, J., Umpierre, A.D., Zhu, J., Bosco, D.B., Dong, H., Wu, L.J., 2019. Neuronal network activity controls microglial process surveillance in awake mice via norepinephrine signaling. Nat. Neurosci. 22, 1771–1781.
Madry, C., Kyrargyri, V., Arancibia-Carcamo, I.L., Jolivet, R., Kohsaka, S., Bryan, R.M., Attwell, D., 2018. Microglial ramification, surveillance, and interleukin-1beta release are regulated by the two-pore domain K(+) channel THIK-1. Neuron 97 299–312.e6.
Mapplebeck, J.C.S., Dalgarno, R., Tu, Y., Moriarty, O., Beggs, S., Kwok, C.H.T., Halievski, K., Assi, S., Mogil, J.S., Trang, T., Salter, M.W., 2018. Microglial P2X4R-evoked pain hypersensitivity is sexually dimorphic in rats. Pain 159, 1752–1763.
Mattei, D., Djodari-IRANI, A., Hadar, R., Pelz, A., De Cossio, L.F., Goetz, T., Matyash, M., Kettenmann, H., Winter, C., Wolf, S.A., 2014. Minocycline rescues decrease in neurogenesis, increase in microglia cytokines and deficits in sensorimotor gating in an animal model of schizophrenia. Brain Behav. Immun. 38, 175–184.
Mccarthy, M.M., Wright, C.L., 2017. Convergence of sex differences and the Neuroimmune system in autism Spectrum disorder. Biol. Psychiatry 81, 402–410.
Michell-Robinson, M.A., Touil, H., Healy, L.M., Owen, D.R., Durafourt, B.A., Bar-Or, A., Antel, J.P., Moore, C.S., 2015. Roles of microglia in brain development, tissue maintenance and repair. Brain 138, 1138–1159.
Morris, S.M., Acosta, M.T., Garg, S., Green, J., Huson, S., Legius, E., North, K.N., Payne, J.M., Plasschaert, E., Frazier, T.W., Weiss, L.A., Zhang, Y., Gutmann, D.H., Constantino, J.N., 2016. Disease burden and symptom structure of autism in neurofibromatosis type 1: a study of the international NF1-ASD consortium team (INFACT). JAMA Psychiatry 73, 1276–1284.
Nelson, L.H., Warden, S., Lenz, K.M., 2017. Sex differences in microglial phagocytosis in the neonatal hippocampus. Brain Behav. Immun. 64, 11–22.
Nimmerjahn, A., Kirchhoff, F., Helmchen, F., 2005. Resting microglial cells are highly dynamic surveillants of brain parenchyma in vivo. Science 308, 1314–1318.
Nissen, J.C., 2017. Microglial function across the Spectrum of age and gender. Int. J. Mol. Sci. 18.
Ousingsawat, J., Wanitchakool, P., Kmit, A., Romao, A.M., Jantarajit, W., Schreiber, R., Kunzelmann, K., 2015. Anoctamin 6 mediates effects essential for innate immunity downstream of P2X7 receptors in macrophages. Nat. Commun. 6, 6245.
Pan, Y., Xiong, M., Chen, R., Ma, Y., Corman, C., Maricos, M., Kindler, U., Semtner, M., Chen, Y.H., Dahiya, S., Gutmann, D.H., 2018. Athymic mice reveal a requirement for T-cell-microglia interactions in establishing a microenvironment supportive of Nf1 low-grade glioma growth. Genes Dev. 32, 491–496.
Pannell, M., Meier, M.A., Szulzewsky, F., Matyash, V., Endres, M., Kronenberg, G., Prinz, V., Waiczies, S., Wolf, S.A., Kettenmann, H., 2016. The subpopulation of microglia expressing functional muscarinic acetylcholine receptors expands in stroke and Alzheimer's disease. Brain Struct. Funct. 221, 1157–1172.
Petrelli, F., Pucci, L., Bezzi, P., 2016. Astrocytes and microglia and their potential link with autism Spectrum disorders. Front. Cell. Neurosci. 10, 21.
Post, S.R., Jacobson, J.P., Insel, P.A., 1996. P2 purinergic receptor agonists enhance cAMP production in Madin-Darby canine kidney epithelial cells via an autocrine/paracrine mechanism. J. Biol. Chem. 271, 2029–2032.
Post, S.R., Rump, L.C., Zambon, A., Hughes, R.J., Buda, M.D., Jacobson, J.P., Kao, C.C., Insel, P.A., 1998. ATP activates cAMP production via multiple purinergic receptors in MDCK-D1 epithelial cells. Blockade of an autocrine/paracrine pathway to define receptor preference of an agonist. J. Biol. Chem. 273, 23093–23097.
Sasmono, R.T., Williams, E., 2012. Generation and characterization of MacGreen mice, the Cfs1r-EGFP transgenic mice. Methods Mol. Biol. 844, 157–176.
Sasmono, R.T., Oceandy, D., Pollard, J.W., Tong, W., Pavli, P., Wainwright, B.J., Ostrowski, M.C., Himes, S.R., Hume, D.A., 2003. A macrophage colony-stimulating factor receptor-green fluorescent protein transgene is expressed throughout the mononuclear phagocyte system of the mouse. Blood 101, 1155–1163.
Schwarz, J.M., Sholar, P.W., Bilbo, S.D., 2012. Sex differences in microglial colonization of the developing rat brain. J. Neurochem. 120, 948–963.
Sorge, R.E., Mapplebeck, J.C., Rosen, S., Beggs, S., Taves, S., Alexander, J.K., Martin, L.J., Austin, J.S., Sotocinal, S.G., Chen, D., Yang, M., Shi, X.Q., Huang, H., Pillon, N.J., Bilan, P.J., Tu, Y., Klip, A., Ji, R.R., Zhang, J., Salter, M.W., Mogil, J.S., 2015. Different immune cells mediate mechanical pain hypersensitivity in male and female mice. Nat. Neurosci. 18, 1081–1083.
Stowell, R.D., Sipe, G.O., Dawes, R.P., Batchelor, H.N., Lordy, K.A., Whitelaw, B.S., Stoessel, M.B., Bidlack, J.M., Brown, E., Sur, M., Majewska, A.K., 2019. Noradrenergic signaling in the wakeful state inhibits microglial surveillance and synaptic plasticity in the mouse visual cortex. Nat. Neurosci. 22, 1782–1792.
Thion, M.S., Low, D., Silvin, A., Chen, J., Grisel, P., Schulte-Schrepping, J., Blecher, R., Ulas, T., Squarzoni, P., Hoeffel, G., Coulpier, F., Siopi, E., David, F.S., Scholz, C., Shihui, F., Lum, J., Amoyo, A.A., Larbi, A., Poidinger, M., Buttgereit, A., Lledo, P.M., Greter, M., Chan, J.K.Y., Amit, I., Beyer, M., Schultze, J.L., Schlitzer, A., Pettersson, S., Ginhoux, F., Garel, S., 2018. Microbiome influences prenatal and adult microglia in a sex-specific manner. Cell 172, 500–516.e16.
Toonen, J.A., Solga, A.C., Ma, Y., Gutmann, D.H., 2017. Estrogen activation of microglia underlies the sexually dimorphic differences in Nf1 optic glioma-induced retinal pathology. J. Exp. Med. 214, 17–25.
Tremblay, M.E., Stevens, B., Sierra, A., Wake, H., Bessis, A., Nimmerjahn, A., 2011. The role of microglia in the healthy brain. J. Neurosci. 31, 16064–16069.
Vanryzin, J.W., Marquardt, A.E., Argue, K.J., Vecchiarelli, H.A., Ashton, S.E., Arambula, S.E., Hill, M.N., Mccarthy, M.M., 2019. Microglial phagocytosis of Newborn cells is induced by Endocannabinoids and sculpts sex differences in juvenile rat social play. Neuron 102, 435–449.e6.
Vegeto, E., Villa, A., Della Torre, S., Crippa, V., Rusmini, P., Cristofani, R., Galbiati, M., Maggi, A., Poletti, A., 2020. The role of sex and sex hormones in neurodegenerative diseases. Endocr. Rev. 41.
Villa, A., Gelosa, P., Castiglioni, L., Cimino, M., Rizzi, N., Pepe, G., Lolli, F., Marcello, E., Sironi, L., Vegeto, E., Maggi, A., 2018. Sex-specific features of microglia from adult mice. Cell Rep. 23, 3501–3511.
Wegscheid, M.L., Anastasaki, C., Gutmann, D.H., 2018. Human stem cell modeling in neurofibromatosis type 1 (NF1). Exp. Neurol. 299, 270–280.
Wendt, S., Maricos, M., Vana, N., Meyer, N., Guneykaya, D., Semtner, M., Kettenmann, H., 2017. Changes in phagocytosis and potassium channel activity in microglia of 5xFAD mice indicate alterations in purinergic signaling in a mouse model of Alzheimer's disease. Neurobiol. Aging 58, 41–53.
Whitelaw, B.S., 2018. Microglia-mediated synaptic elimination in neuronal development and disease. J. Neurophysiol. 119, 1–4.

Wolf, S.A., Boddeke, H.W., Kettenmann, H., 2017. Microglia in physiology and disease. Annu. Rev. Physiol. 79, 619–643.
Wright-Jin, E.C., Gutmann, D.H., 2019. Microglia as dynamic cellular mediators of brain function. Trends Mol. Med. 25, 967–979.
Xu, Y., Hu, W., Liu, Y., Xu, P., Li, Z., Wu, R., Shi, X., Tang, Y., 2016. P2Y6 receptor-mediated microglial phagocytosis in radiation-induced brain injury. Mol. Neurobiol. 53, 3552–3564.
Yirmiya, R., Rimmerman, N., Reshef, R., 2015. Depression as a microglial disease. Trends Neurosci. 38, 637–658.